

# Segmentation-Based Attention Entropy: Detecting and Mitigating Object Hallucinations in Large Vision-Language Models

Jiale Song, Jiaxin Luo, Xue-song Tang, Kuangrong Hao, Mingbo Zhao

School of Information and Intelligent Science, Donghua University, Shanghai, 201620, China

2222026@mail.dhu.edu.cn, 1249118@mail.dhu.edu.cn, tangxs@dhu.edu.cn, krhao@dhu.edu.cn, mzhao4@dhu.edu.cn

**Abstract**—Large Vision-Language Models (LVLMs) achieve strong performance on many multimodal tasks, but object hallucinations severely undermine their reliability. Most existing studies focus on the text modality, attributing hallucinations to overly strong language priors and insufficient visual grounding. In contrast, we observe that abnormal attention patterns within the visual modality can also give rise to hallucinated objects. Building on this observation, we propose Segmentation-based Attention Entropy (SAE), which leverages semantic segmentation to quantify visual attention uncertainty in an object-level semantic space. Based on SAE, we further design a reliability score for hallucination detection and an SAE-guided attention adjustment method that modifies visual attention at inference time to mitigate hallucinations. We evaluate our approach on public benchmarks and in real embodied multimodal scenarios with quadruped robots. Experimental results show that SAE substantially reduces object hallucinations without any additional training cost, thereby enabling more trustworthy LVLM-driven perception and decision-making.

**Index Terms**—Large vision-language models, Object hallucinations, Uncertainty estimation, Embodied navigation

## I. INTRODUCTION

Large Vision-Language Models (LVLMs) have achieved strong performance on image captioning, visual question answering, multimodal dialogue, and embodied robotic perception [1]–[3]. However, they still suffer severely from hallucinations, especially object hallucinations where the model describes objects that do not exist in the image [4], [5].

To mitigate hallucinations in LVLMs, prior work has explored robust visual instruction tuning for better multimodal alignment [6], [7], as well as training-free decoding strategies such as Visual Contrastive Decoding (VCD) [8]. Other studies further analyze the causes of object hallucinations and conclude that language bias is a primary factor [9]–[11]. Recently, some work has begun to investigate visual-side internal mechanisms in LVLMs [12], but it does not explicitly characterize the uncertainty of visual attention at the semantic object level.

As illustrated in Fig. 1, when an LVLM generates a description, its attention should focus on image regions that are semantically consistent with the target object, rather than being diffused over many irrelevant areas. In practice, regions where visual attention is highly dispersed and which therefore exhibit high attention uncertainty are more likely to give rise to hallucinations.

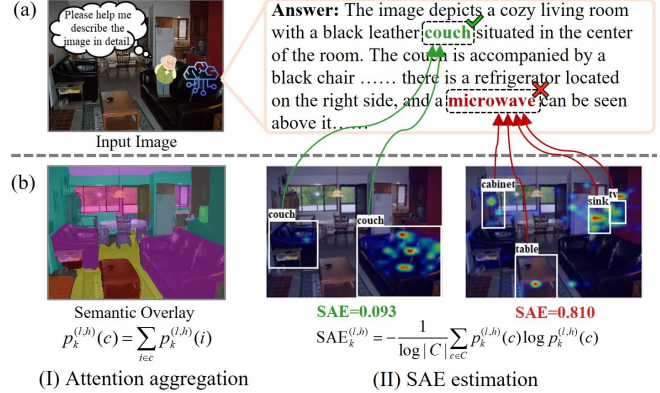


Fig. 1. Object hallucinations in LVLMs and SAE. (a) Example of real (green) and hallucinated (red) objects in an LVLM description. (b) SAE pipeline: real objects correspond to low SAE, hallucinated objects to high SAE.

Motivated by this, we propose Segmentation-based Attention Entropy (SAE) to characterize the uncertainty of visual attention inside LVLMs from an object-level semantic perspective. As shown in Fig. 1(b), we first apply a semantic segmentation model to the input image, aggregate visual-token attention according to semantic categories, and then compute a normalized entropy over the category-level attention distribution to measure how dispersed the attention is over different semantic regions. Empirically, when predicting tokens corresponding to real objects, attention concentrates on semantically consistent regions, leading to low SAE; hallucinated objects, instead, show attention drifting to irrelevant regions and thus significantly higher SAE.

Building on this observation, we construct a reliability score that combines cross-modal attention quality with SAE for object-level hallucination detection, and design an SAE-guided modulation strategy that directly adjusts attention logits during inference, mitigating object hallucinations without any additional training cost.

The main contributions of this paper are summarized as follows:

- We propose SAE, which quantifies the uncertainty of LVLM visual attention at the object level via semantic segmentation, turning the question of whether attention focuses on semantically consistent regions into a com-

putable entropy metric.

- We reveal a correlation between SAE and object hallucinations, and accordingly introduce an attention reliability score that fuses cross-modal attention quality with SAE for object-level hallucination detection.
- We develop an SAE-guided inference-time attention modulation method that reshapes visual attention without modifying model parameters, significantly reducing CHAIR hallucination rates on COCO and in embodied scenarios with quadruped robots, and improving the reliability of LVLM-based perception and decision-making.

## II. METHOD

### A. Preliminaries

**Notation and attention.** We discretize the input image into  $n$  visual tokens  $v_{1:n}$  and the instruction into  $m$  text tokens  $t_{1:m}$ . At decoding step  $k$ , the input prefix to the language model is given by  $x_{1:a_k} = (v_{1:n}, t_{1:m}, y_{1:k-1})$ , where  $a_k = n+m+k-1$ . The model then predicts the next token  $y_k$  at this step. Let  $L$  denote the number of Transformer layers and  $H$  the number of attention heads. We denote by  $A_k^{(l,h)} \in \mathbb{R}^{a_k \times a_k}$  the attention matrix at layer  $l \in [L]$  and head  $h \in [H]$  for step  $k$ , where  $a_k$  is the prefix length. In particular, the entry  $A_k^{(l,h)}(a_k, i)$  represents the attention weight assigned by the newly generated token  $y_k$  to the  $i$ -th token in the prefix. When  $i$  corresponds to a visual token  $v_i$ ,  $A_k^{(l,h)}(a_k, i)$  measures how much attention  $y_k$  places on the  $i$ -th visual token.

**Background on uncertainty estimation.** In information theory, Shannon entropy is used to quantify the uncertainty of a discrete distribution. Given a discrete random variable with probability vector  $p = (p_1, \dots, p_K)$ , its Shannon entropy is defined as

$$H(p) = - \sum_{i=1}^K p_i \log p_i. \quad (1)$$

Existing research typically relates the uncertainty of large language models (LLMs) to hallucinations and employs entropy-based uncertainty measures to detect hallucinated outputs [13]. In the context of LVLMs, however, the allocation of attention in multimodal interactions is particularly crucial [12], yet prior work tends to focus more on the text modality while paying insufficient attention to the image modality [9], [10]. Inspired by these studies, we observe that SAE can be used to quantify the uncertainty of attention distributions within the image modality, which in turn can be exploited to detect and mitigate hallucinations in LVLMs.

### B. Segmentation-based Attention Entropy

**Semantic uncertainty in images.** If we simply treat, for each generated text token, the attention weights over all visual tokens as a probability distribution, we inevitably mix two different sources of uncertainty: (i) the uncertainty over the underlying visual semantics, and (ii) the uncertainty induced by the number and size of the tokenized instances that express those semantics. For example, when a high-confidence object is present in the image, it may correspond either to

a single large region covered by many visual tokens or to multiple smaller instances. In this case, a spread-out attention distribution over visual tokens does not necessarily indicate semantic ambiguity, but may instead reflect the spatial extent or multiplicity of the object.

Our method aims to estimate the uncertainty of the LVLMs' attention over visual semantics when generating a text-level object token, rather than over the number or size of its visual instances. Therefore, we first cluster visual tokens according to semantic segments and then compute attention uncertainty on top of these clusters. Specifically, the procedure consists of the following two steps:

#### (I) Attention aggregation

For the  $k$ -th generated token  $y_k$ , recall that the attention weight assigned to visual token  $v_i$  at layer  $l$  and head  $h$  is  $A_k^{(l,h)}(a_k, i)$ . We normalize the attention over visual tokens to obtain a probability distribution:

$$p_k^{(l,h)}(i) = \frac{A_k^{(l,h)}(a_k, i)}{\sum_{j=1}^n A_k^{(l,h)}(a_k, j)}, \quad i \in \{1, \dots, n\}. \quad (2)$$

To group visual tokens by object-level semantics, we apply Mask2Former-Swin-L [14] to perform semantic segmentation on the image, obtaining  $|C|$  disjoint semantic classes. We assign each visual token the semantic label that occupies the largest number of pixels within its receptive region. For a semantic class  $c \in C$ , we aggregate the probabilities of all visual tokens belonging to that class to obtain a class-level distribution:

$$p_k^{(l,h)}(c) = \sum_{i \in c} p_k^{(l,h)}(i). \quad (3)$$

In other words, the attention probabilities of all tokens corresponding to the same object category (possibly spanning multiple instances and sizes) are pooled into a single semantic class.

#### (II) SAE estimation

Given the class-level attention distribution in (3), we define the SAE as:

$$\text{SAE}_k^{(l,h)} = - \frac{1}{\log |C|} \sum_{c \in C} p_k^{(l,h)}(c) \log p_k^{(l,h)}(c). \quad (4)$$

This quantity measures how dispersed the attention is across different semantic segmentation classes when predicting  $y_k$ . To make SAE comparable across images with different numbers of semantic classes, we normalize by the maximum entropy  $\log |C|$ , so that  $\text{SAE}_k^{(l,h)} \in [0, 1]$ .

### C. Object-level Uncertainty Estimation with SAE

**Empirical observations and intuition.** We are interested in whether real and hallucinated objects exhibit systematic differences in their attention distributions within the visual modality. According to the SAE defined in Sec. II-B, when the attention used to predict an object token is more dispersed across semantic segmentation classes, the corresponding SAE is higher, indicating that the visual evidence is less concentrated and the semantic uncertainty is higher, which in turn suggests a higher risk of hallucination.

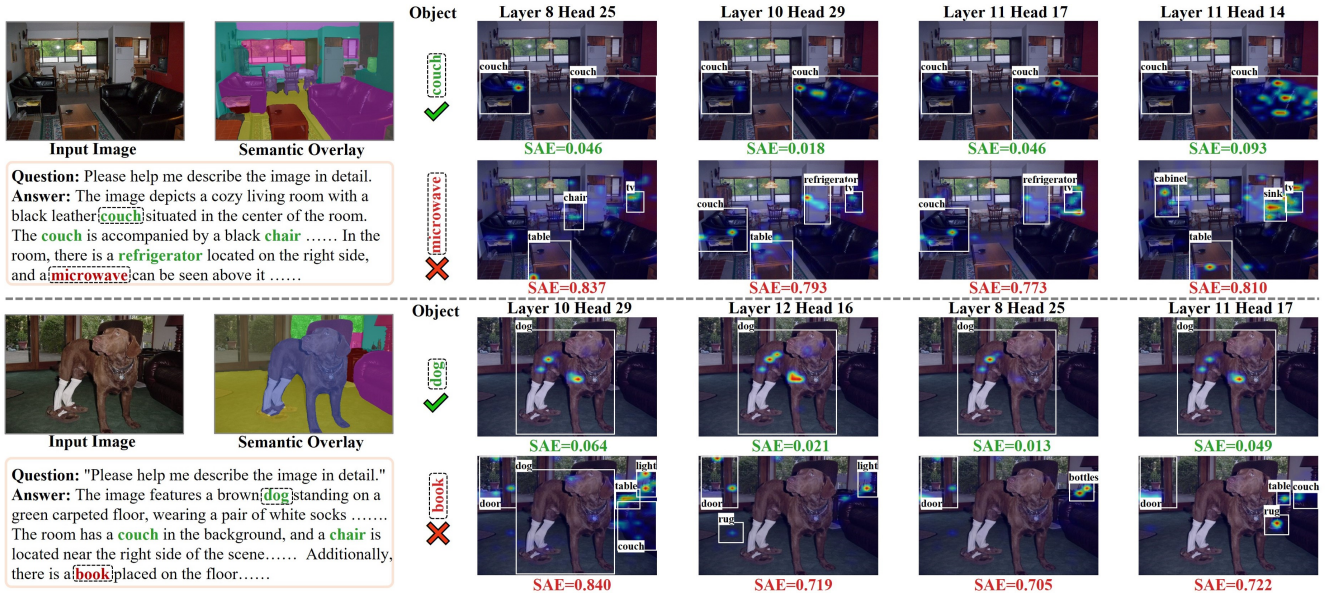


Fig. 2. Head-level attention distributions for real objects (green) and hallucinated objects (red). Real objects have low SAE with attention concentrated on the corresponding image tokens, whereas hallucinated objects have high SAE with attention spread over many irrelevant image tokens.

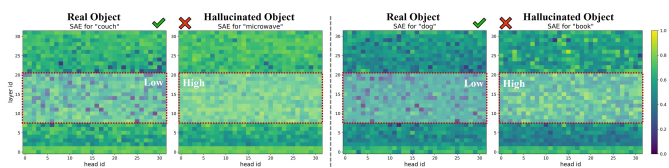


Fig. 3. Layer-head SAE statistics. The horizontal axis denotes the head index and the vertical axis the layer index, and the difference between real and hallucinated objects is most pronounced in the middle layers.

Fig. 2 visualizes attention heatmaps and the associated SAE values for several attention heads. When attention mainly focuses on the sofa or dog regions, the SAE values are low; when attention drifts across multiple unrelated regions, SAE becomes much larger. This aligns with our intuition: the more dispersed the attention, the higher the SAE and the greater the hallucination risk.

Fig. 3 shows SAE values aggregated over all layers and heads of LLaVA-1.5-7B for the real and hallucinated objects in the two examples of Fig. 2. A consistent pattern emerges across layer-head pairs: real objects tend to have lower SAE, while hallucinated objects exhibit higher SAE. The gap is most pronounced in the intermediate layers: early layers mainly capture low-level and coarse-grained representations, while very late layers are dominated by language modeling, so the difference diminishes again.

**Summary and usage.** Based on the above observations, we treat SAE as a signal that is complementary to cross-modal attention quality for hallucination detection. Specifically, together with SAE we compute, for the same layer-head, the total attention mass from the text-level object token to all visual tokens, and define an attention reliability score as:

$$R_k^{(l,h)} = M_k^{(l,h)}(1 - \text{SAE}_k^{(l,h)}), \quad (5)$$

where  $M_k^{(l,h)}$  is the attention mass, that is the sum of attention weights from the object token to all visual tokens, and  $R_k^{(l,h)}$  captures the reliability of both cross-modal and intra-modal attention. Intuitively, a high  $R_k^{(l,h)}$  indicates that the model is looking at the image in a focused and confident manner. Following the empirical pattern observed in Fig. 3 and the middle-layer design in VAR [12], we aggregate the reliability scores by first averaging  $R_k^{(l,h)}$  over the middle layers for each head, and then averaging the resulting values over all attention heads to obtain a scalar score for hallucination detection.

#### D. SAE-guided Object Hallucination Mitigation

Sec. II-C shows that the more dispersed the attention used to predict an object token is across semantic segmentation classes, the higher the corresponding SAE, and the more likely the token is to be hallucinated. To reduce the hallucination rate of the model, we therefore aim to adjust the attention distribution over visual tokens so that the model focuses more on the true object regions rather than spreading attention across unrelated areas.

We design an SAE-guided attention modulation strategy that intervenes in the attention scores (pre-softmax logits) during inference. Let  $S_k^{(l,h)}(a_k, i)$  denote the pre-softmax attention logit at decoding step  $k$  from the query position  $a_k$  to the  $i$ -th visual token at layer  $l$  and head  $h$ , where  $i \in \{1, \dots, n\}$ . We then construct an attention consistency map by taking the absolute values of these logits and averaging them over heads:

$$C_k^{(l)}(i) = \frac{1}{H} \sum_{h=1}^H |S_k^{(l,h)}(a_k, i)|, \quad i \in \{1, \dots, n\}. \quad (6)$$

For each head, we then compute its SAE at step  $k$  and use it as a linear gate to determine a head-specific enhancement

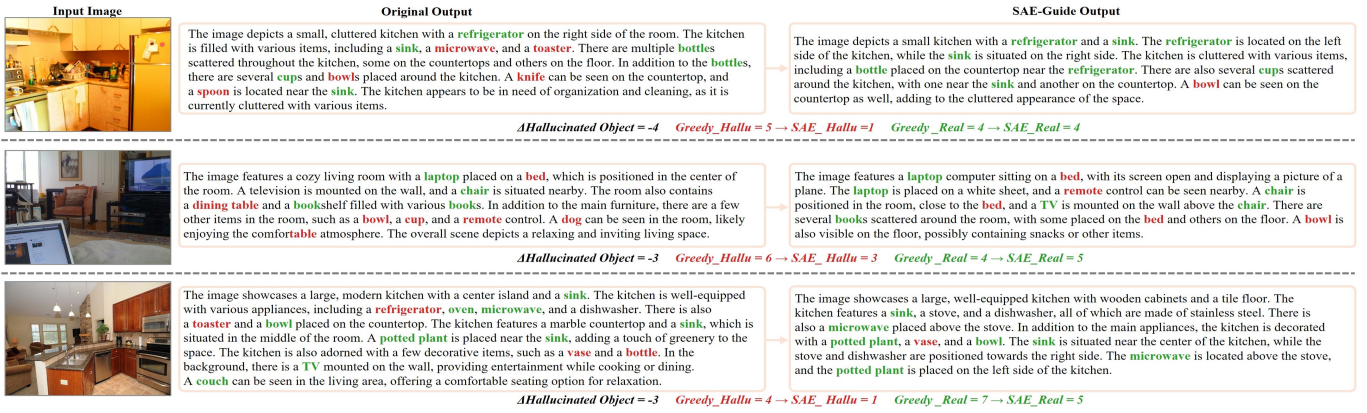


Fig. 4. Qualitative example of SAE-guided attention intervention during inference. SAE-guided modulation reduces hallucinated objects (red) such as a spoon, a dining table, and a dog, while preserving or even completing real objects (green).

strength:

$$\tilde{S}_k^{(l,h)}(a_k, i) = S_k^{(l,h)}(a_k, i) + \lambda \text{SAE}_k^{(l,h)} C_k^{(l)}(i), \quad (7)$$

where  $\lambda$  is an intervention coefficient (set to 0.5 by default). In other words, we use SAE to dynamically modulate the strength of attention consistency enhancement for each head: heads with higher SAE (more uncertain intra-modal attention) are more strongly nudged towards the consensus pattern  $C_k^{(l)}$ , resulting in a more focused attention distribution over visual tokens.

Fig. 4 presents a qualitative example of SAE-guided attention intervention. Without intervention (greedy decoding), the model produces hallucinated objects absent from the image. After SAE-guided modulation, most hallucinations are removed or replaced, with real objects better preserved or completed. Correspondingly, hallucinated objects decrease while real objects remain roughly unchanged, indicating that SAE-guided intervention effectively focuses attention on image-consistent regions and substantially suppresses object hallucinations without sacrificing description richness.

### E. SAE-guided Navigation for Embodied Agents

LVLMS have been widely applied to embodied intelligence and robot navigation [3], [15], but most systems overlook the hallucination issue, which may lead to navigation failures or incorrect decisions. To address this, we apply SAE to an LVLMS-based navigation scenario using a quadruped robot equipped with an RGB-D camera and a LiDAR.

The overall pipeline is illustrated in Fig. 5. The robot receives a first-person image and a high-level instruction, and a navigation prompt guides the LVLMS to describe the scene and output one or more navigation target objects. Vanilla LVLMS are prone to hallucinations, often producing incorrect target objects or vague “explore again” instructions. To mitigate this problem, we adopt the method proposed in Sec. II-D to reduce output hallucinations. Subsequently, the predicted navigation targets are grounded in the image using YOLO-World [16], an open-vocabulary object detection model. For each textual label, YOLO-World returns a corresponding bounding box,

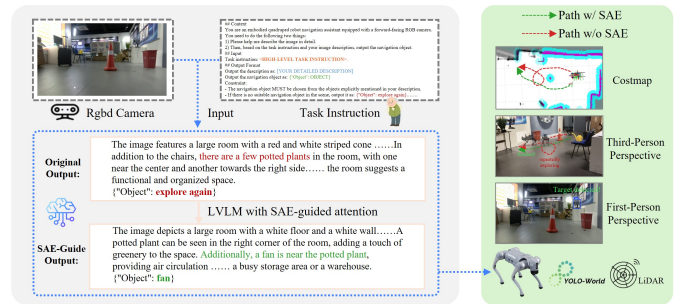


Fig. 5. SAE-Guided Navigation Pipeline: The robot takes a first-person RGB-D image and a language instruction as inputs to the LVLMS, with the output being an action path in the physical world.

which is projected into the robot’s coordinate system with depth information and mapped onto a LiDAR-based local costmap as a navigation waypoint. Finally, the local planner generates a collision-free path from the current pose to the target waypoint on the costmap. This pipeline converts potentially hallucination-prone LVLMS predictions into a more reliable object-level navigation decision-making process.

## III. EXPERIMENTS

In this section, we conduct a systematic quantitative evaluation of the proposed method, including three parts: hallucination detection (Sec. III-A), hallucination mitigation (Sec. III-B), and LVLMS-based navigation (Sec. III-C).

### A. Hallucination Detection

**Experimental setup.** We evaluate two open-source LVLMS: LLaVA-1.5-7B and LLaVA-1.5-13B. We randomly sample 1,000 images from the COCO 2014 validation set and let the models generate descriptions. For each image, we extract all object tokens in the generated text and label them as real if the object appears in the COCO annotation of that image and hallucinated otherwise. The basic detection unit is therefore the object token. Real object tokens are treated as positive examples, and hallucinated object tokens as negative examples.

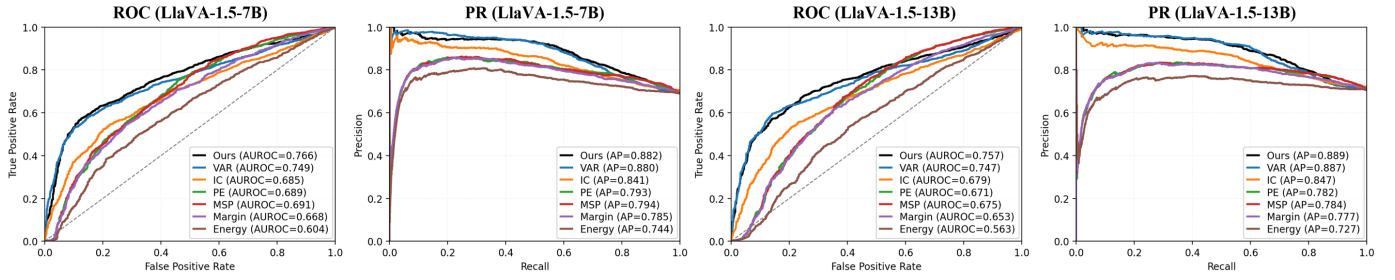


Fig. 6. ROC and PR curves of different hallucination detection methods on LLaVA-1.5-7B and LLaVA-1.5-13B.

For our approach, we use the SAE-based reliability score  $R$  defined in Sec. II-C as the detection score.

**Evaluation metrics.** We evaluate hallucination detection using AUROC and AP, and report ROC and PR curves.

**Baselines.** We compare standard uncertainty-based hallucination detection scores: predictive entropy (PE) [17], maximum softmax probability (MSP) [18], margin [19], energy score [20], internal confidence (IC) [21], and the Visual Attention Ratio (VAR) [12], following original implementations.

Fig. 6 shows that our method consistently outperforms all baselines on both models, especially at low false-positive rates and in the high-recall regime. From the AUROC/AP values reported in the figure, we can see that on LLaVA-1.5-7B our method achieves 0.766/0.882 compared to 0.749/0.880 for the strongest baseline VAR, and on LLaVA-1.5-13B the scores improve from 0.747/0.887 (VAR) to 0.757/0.889. Compared with output-distribution-based uncertainty measures (PE, MSP, Margin, Energy), our approach improves AUROC by about 7–15 percentage points and also yields clear gains in AP. These results indicate that modeling intra-visual uncertainty via SAE provides a more discriminative signal for distinguishing hallucinated from real objects.

### B. Hallucination Mitigation

**Experimental setup.** We reuse the two LVLMs and the COCO 2014 setup from Sec. III-A. Decoding temperature, maximum generation length, and other hyperparameters are kept identical across methods, and all methods use the same prompts. Our method applies the SAE-guided inference-time attention intervention described in Sec. II-D.

**Evaluation metrics.** We use CHAIR [4] to quantify caption-level object hallucinations, reporting sentence-level ( $C_S$ ) and instance-level ( $C_I$ ) rates; lower is better. Following prior work, we also compute object-level precision, recall, and F1 with ground-truth objects as positives.

**Baselines.** We consider three standard decoding strategies: greedy decoding, beam search [22], and nucleus (top- $p$ ) sampling [23]. We also evaluate four inference-time hallucination mitigation methods: OPERA [9], VCD [8], PAI [10], and VAR [12], all applied on top of greedy decoding.

Tab. I shows the upper block as decoding strategies and the lower as inference-time interventions. Our method achieves lowest or tied-for-lowest sentence- and instance-level hallucination rates  $C_S$  and  $C_I$  on both models with F1 close to

TABLE I  
CHAIR AND P/R/F1 RESULTS OF DIFFERENT METHODS ON LLaVA-1.5-7B AND LLaVA-1.5-13B (MAX LENGTH = 512).

Method	LLaVA-1.5-7B					LLaVA-1.5-13B					Avg	
	$C_S \downarrow$	$C_I \downarrow$	R $\uparrow$	P $\uparrow$	F1 $\uparrow$	$C_S \downarrow$	$C_I \downarrow$	R $\uparrow$	P $\uparrow$	F1 $\uparrow$	$C_S \downarrow$	$C_I \downarrow$
Nucleus	56.0	16.4	73.4	71.0	72.2	54.0	15.0	74.6	73.0	73.8	55.0	15.7
Greedy	47.9	13.6	78.1	75.8	77.0	44.3	11.7	77.6	78.7	<b>78.2</b>	46.1	12.6
Beam	52.1	14.1	<b>78.5</b>	75.2	76.8	49.7	12.7	<b>79.1</b>	77.3	<b>78.2</b>	50.9	13.4
OPERA	48.5	13.7	78.1	75.5	76.8	52.6	14.1	68.1	73.1	70.5	50.6	13.9
VCD	55.4	15.7	75.6	71.8	73.7	52.3	13.9	75.5	74.6	75.1	53.8	14.8
PAI	30.1	8.8	70.8	83.7	76.7	28.9	<b>8.5</b>	70.4	83.4	76.4	29.5	8.6
VAR	25.3	6.5	69.2	86.6	<b>76.9</b>	26.7	8.8	67.3	84.1	74.7	26.0	7.6
Ours	<b>24.2</b>	<b>5.9</b>	68.2	<b>87.3</b>	76.6	<b>23.8</b>	<b>8.5</b>	64.8	<b>85.9</b>	73.9	<b>24.0</b>	<b>7.2</b>

the best baselines. On LLaVA-1.5-7B, greedy decoding yields  $C_S/C_I$  of 47.9/13.6, whereas our method reduces them to 24.2/5.9, roughly halving hallucinations; on LLaVA-1.5-13B,  $C_S$  similarly drops from 44.3 to 23.8. Overall, SAE-guided attention intervention provides the best average  $C_S$  and  $C_I$  with only a small F1 loss, achieving a favorable trade-off between low hallucination and high accuracy.

### C. LVLm-based Navigation

**Scene setup.** We conducted experiments in complex indoor environments using a Unitree Go1 quadruped robot. The robot is equipped with an RGB-D camera and a LiDAR, with LLaVA-1.5-7B and YOLO-World employed as the perception and decision-making module and image grounding modules, respectively. Detection results, depth images, and LiDAR scan data are fused to generate a costmap, which the robot uses for path planning.

As shown in Fig. 7, in the single-target scenario, target hallucinations prevent the LVLm from accurately perceiving the navigation goal. The robot repeats exploration and must approach the target at an extremely close distance to achieve successful navigation. After mitigating hallucinations, the LVLm focuses on the correct target earlier, leading to a significant reduction in navigation time. In the multi-target scenario, the baseline method only predicts the plant as a target and misclassifies the watering can as a toy, resulting in missing navigation targets and failing to fulfill the task as instructed. With hallucinations mitigated, the LVLm can recognize both the watering can and the plant as sequential targets. The planner generates two paths on the costmap: the

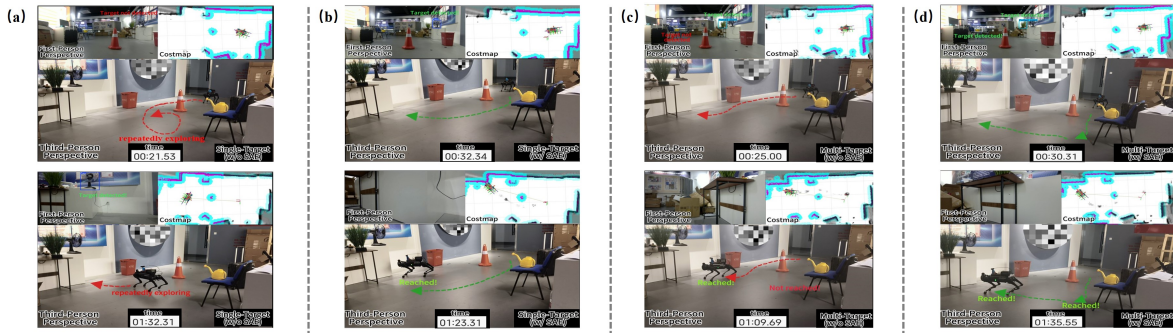


Fig. 7. Comparison of LVLM-based navigation in single-target and multi-target scenarios with and without SAE (details in the supplementary video).

robot first moves to the watering can and then to the plant, achieving multi-step navigation consistent with the instruction. These results demonstrate that SAE effectively reduces target hallucinations, making navigation behavior more semantically consistent and efficient.

#### IV. CONCLUSION

We propose SAE to quantify the uncertainty of visual attention at the object level and show that it is strongly correlated with object hallucinations in LVLMs. Building on SAE, we design a reliability score for object-level hallucination detection and an inference-time attention modulation strategy that significantly reduces CHAIR hallucination rates without additional training cost, and we further validate its effectiveness on COCO and in quadruped-robot scenarios. In future work, we plan to apply SAE to a wider range of multimodal and embodied tasks in order to further improve the reliability of LVLMs in real-world settings.

#### REFERENCES

- [1] Haotian Liu, Chunyuan Li, Qingyang Wu, and Yong Jae Lee, “Visual instruction tuning,” in *Advances in Neural Information Processing Systems*, 2023.
- [2] Junnan Li, Dongxu Li, Silvio Savarese, and Steven Hoi, “Blip-2: Bootstrapping language-image pre-training with frozen image encoders and large language models,” in *International conference on machine learning*. PMLR, 2023, pp. 19730–19742.
- [3] Jing Gu, Eliana Stefani, Qi Wu, Jesse Thomason, and Xin Wang, “Vision-and-language navigation: A survey of tasks, methods, and future directions,” in *Proceedings of the 60th Annual Meeting of the Association for Computational Linguistics (Volume 1: Long Papers)*, 2022, pp. 7606–7623.
- [4] Anna Rohrbach, Lisa Anne Hendricks, Kaylee Burns, Trevor Darrell, and Kate Saenko, “Object hallucination in image captioning,” in *Proceedings of the 2018 Conference on Empirical Methods in Natural Language Processing*, 2018, pp. 4035–4045.
- [5] Yifan Li, Yifan Du, Kun Zhou, Jinpeng Wang, Wayne Xin Zhao, and Ji-Rong Wen, “Evaluating object hallucination in large vision-language models,” in *Proceedings of the 2023 Conference on Empirical Methods in Natural Language Processing*, 2023, pp. 292–305.
- [6] Fuxiao Liu, Kevin Lin, Linjie Li, Jianfeng Wang, Yaser Yacoob, and Lijuan Wang, “Mitigating hallucination in large multi-modal models via robust instruction tuning,” in *Proceedings of the International Conference on Learning Representations*, 2024.
- [7] Chaoya Jiang, Haiyang Xu, Mengfan Dong, Jiaying Chen, Wei Ye, Ming Yan, Qinghao Ye, Ji Zhang, Fei Huang, and Shikun Zhang, “Hallucination augmented contrastive learning for multimodal large language model,” in *Proceedings of the IEEE/CVF Conference on Computer Vision and Pattern Recognition*, 2024, pp. 27036–27046.
- [8] Shaohan Leng, Hong Zhang, Guanting Chen, Xinzhe Li, Shuming Lu, Chunyan Miao, and Lidong Bing, “Mitigating object hallucinations in large vision-language models through visual contrastive decoding,” in *Proceedings of the IEEE/CVF Conference on Computer Vision and Pattern Recognition*, 2024.
- [9] Qi Huang, Xiaoyi Dong, Peng Zhang, Bo Wang, Changkun He, Jingdong Wang, Dahua Lin, Wenqi Zhang, and Nanning Yu, “Opera: Alleviating hallucination in multi-modal large language models via over-trust penalty and retrospection-allocation,” in *Proceedings of the IEEE/CVF Conference on Computer Vision and Pattern Recognition*, 2024.
- [10] Shi Liu, Kecheng Zheng, and Wei Chen, “Paying more attention to image: A training-free method for alleviating hallucination in lvm,” in *European Conference on Computer Vision*. Springer, 2024, pp. 125–140.
- [11] Hanchao Liu, Wenyuan Xue, Yifei Chen, Dapeng Chen, Xiutian Zhao, Ke Wang, Liping Hou, Rongjun Li, and Wei Peng, “A survey on hallucination in large vision-language models,” *CoRR*, 2024.
- [12] Zhangqi Jiang, Junkai Chen, Beier Zhu, Tingjin Luo, Yankun Shen, and Xu Yang, “Devils in middle layers of large vision-language models: Interpreting, detecting and mitigating object hallucinations via attention lens,” in *Proceedings of the Computer Vision and Pattern Recognition Conference*, 2025, pp. 25004–25014.
- [13] Sebastian Farquhar, Jannik Kossen, Lorenz Kuhn, and Yarin Gal, “Detecting hallucinations in large language models using semantic entropy,” *Nature*, vol. 630, no. 8017, pp. 625–630, 2024.
- [14] Bowen Cheng, Ishan Misra, Alexander G Schwing, Alexander Kirillov, and Rohit Girdhar, “Masked-attention mask transformer for universal image segmentation,” in *Proceedings of the IEEE/CVF conference on computer vision and pattern recognition*, 2022, pp. 1290–1299.
- [15] Weiqin Zu, Wenbin Song, Ruiqing Chen, Ze Guo, Fanglei Sun, Zheng Tian, Wei Pan, and Jun Wang, “Language and sketching: An llm-driven interactive multimodal multitask robot navigation framework,” in *2024 IEEE International Conference on Robotics and Automation (ICRA)*. IEEE, 2024, pp. 1019–1025.
- [16] Tianheng Cheng, Lin Song, Yixiao Ge, Wenyu Liu, Xinggang Wang, and Ying Shan, “Yolo-world: Real-time open-vocabulary object detection,” in *Proceedings of the IEEE/CVF conference on computer vision and pattern recognition*, 2024, pp. 16901–16911.
- [17] Qing Li, Jiahui Geng, Chenyang Lyu, Derui Zhu, Maxim Panov, and Fakhri Karray, “Reference-free hallucination detection for large vision-language models,” in *Findings of the Association for Computational Linguistics: EMNLP 2024*, 2024, pp. 4542–4551.
- [18] Dan Hendrycks and Kevin Gimpel, “A baseline for detecting misclassified and out-of-distribution examples in neural networks,” in *International Conference on Learning Representations*, 2017.
- [19] Lakpa Tamang et al., “Margin-bounded confidence scores for out-of-distribution detection,” in *Proceedings of the IEEE International Conference on Data Mining (ICDM)*, 2024.
- [20] Weitang Liu, Xiaoyun Wang, John D. Owens, and Yixuan Li, “Energy-based out-of-distribution detection,” in *Advances in Neural Information Processing Systems*, 2020.
- [21] N. Jiang, A. Kachintaya, S. Petyrk, Y. Gandelsman, et al., “Interpreting and editing vision-language representations to mitigate hallucinations,” in *International Conference on Learning Representations*, 2025.
- [22] Ilya Sutskever, Oriol Vinyals, and Quoc V. Le, “Sequence to sequence

learning with neural networks,” in *Advances in Neural Information Processing Systems*, 2014.

- [23] Ari Holtzman, Jan Buys, Li Du, Maxwell Forbes, and Yejin Choi, “The curious case of neural text degeneration,” in *International Conference on Learning Representations*, 2020.